# Formation of porous calcite mesocrystals from $CO_2$–$H_2O$–$Ca(OH)_2$ slurry in the presence of common domestic drinks

G. Montes-Hernandez,*[ab] F. Renard,[abc] N. Findling[ab] and A.-L. Auzende[bd]

This study reports a simple, innovative and fast method to synthesize porous calcite mesocrystals with high specific surface area from $Ca(OH)_2$–water–$CO_2$ slurry in the presence of common domestic drinks (soluble coffee, orange juice, carrot juice, white wine, sugar–water and milk). As already reported in previous studies, calcite nanoparticles (<100 nm) can be obtained at low temperature (≤30 °C) in the absence of additives. We demonstrate herein that the use of common domestic drinks as additives can induce the formation of calcite mesocrystals with a peanut-like morphology, *i.e.* the formation of a nanostructured material in which the constituent calcite nanoparticles (10 < size < 50 nm) are aligned and/or oriented, forming regular micrometric (<3 μm) 3D porous aggregates. We note that the additives used in the system did not induce polymorphism because only calcite was measured/observed in the solid products using XRD, FESEM and TEM or in collected-time suspensions using Raman spectroscopy. This innovative method for synthesizing porous calcite mesocrystals has significant relevance because only a few hours (6 h < time < 24 h) were required and synthesis was possible using a dispersed triphasic gas–liquid–solid system under high non-constant $CO_2$ pressure (anisobaric conditions), contrary to available methods requiring days or weeks, in which reactant diffusion is typically imposed since these systems were initially designed to mimic biomineralization processes. Moreover, this new synthesis method could easily be scaled to industrial processes to produce calcite mesocrystals with high specific surface area (up to 30 $m^2$ $g^{-1}$). The nanostructured state, the mesoporosity and the high specific surface area for these synthesized calcite mesocrystals could improve the typical industrial and medical uses for synthetic calcite.

## 1. Introduction

The biotic and abiotic formation of carbonates plays a crucial role in the global carbon cycle. In addition, carbonate minerals often sequester various trace elements (actinides and lanthanides), metalloids, and heavy metals, and thus control in part their global cycling. Particularly, calcium carbonates are the key structural components of many bio-minerals in invertebrates such as seashells and corals. Calcite is the most common carbonate, shaping the surface of the Earth in many sedimentary basins and mountain ranges in the form of limestones and marbles.[1–3] Understanding how calcite can nucleate and grow represents crucial challenges addressed since the 1970s,[4,5] including processes of biomineralization.[6] However, calcite nucleation and growth processes, including the

influence of foreign impurities and additives, are still a debated subject. On the basis of recent experimental studies, particularly for aqueous systems, calcite can be formed following classical crystallization pathways, *i.e.* spontaneous nucleation from supersaturated solutions or heterogeneous nucleation on pre-existing nucleation sites followed by crystal growth occurring *via* ion-by-ion or molecule-by-molecule addition to existing nuclei.[7–10] Typically, in such cases, single crystals (nano-sized, sub-micrometric or micrometric) with scalenohedral or rhombohedral morphology are obtained.[11] More recently, various studies have also demonstrated that calcite can be formed following the so-called non-classical crystallization pathway. This more complex pathway (in homogeneous systems) involves firstly the formation of stable clusters "pre-nucleation clusters" from ionic solution,[12] early identified as "polymer-induced liquid precursors."[13] Following this non-classical concept, the clusters are aggregated/organized to form amorphous and/or crystalline calcium carbonate or amorphous bulk phase nucleation followed by its rapid transformation into crystalline bulk phase.[14] Finally, the mesoscale self-assembly of primary nanoparticles or units forming often the so-called mesocrystals can be also

[a] *CNRS, ISTerre, F-38041 Grenoble, France.*
*E-mail: german.montes-hernandez@ujf-grenoble.fr*
[b] *Univ. Grenoble Alpes, ISTerre, F-38041 Grenoble, France*
[c] *PGP, University of Oslo, Box 1048 Blindern, 0316 Oslo, Norway*
[d] *Institut de minéralogie et de physique des milieux condensés (IMPMC), CNRS-UPD-UPMC, 4 place Jussieu, 75252 Paris, France*

considered in this non-classical crystallization pathway.[15] The mesocrystals of calcite obtained in this way can be finally metamorphosed by crystallographic fusion into single crystals, containing macromolecules in their structure.[15–17] Recent studies claim that ACC nanoparticles do not necessarily serve as direct precursors to calcite nucleation.[8,9,18] By definition, mesocrystals are nanostructured materials in which the constituent non-spherical nanoparticles (<100 nm) are aligned and/or oriented, forming regular sub-micrometric or micrometric 2D or 3D aggregates that are often porous or non-porous if organic molecules completely fill the existing space between the primary nanoparticles.[19] Mesocrystals have therefore been drawing rapidly increasing attention from chemists and physicists in recent years because they offer unique new opportunities for designing materials due to their mesoscopic structure.[17,20]

Limestone, the most common natural rock that contains mainly calcite, has extensive industrial applications: it is the main component of concretes and several raw building materials. However, the actual usefulness of calcite and other calcium carbonate polymorphs extends far beyond the current usages to which limestone is put. Industrial applications of calcite are mainly determined by textural properties, such as average particle size, particle size distribution, morphology, specific surface area and aggregation state.[21] In this way, porous calcite mesocrystals with a high specific surface area could offer new possibilities for use that have been little explored so far. We note that the calcite mesocrystals have been mainly obtained in the presence of organic additives (particularly macromolecules) such as soluble polymers, polysaccharides and proteins[7,22–25] or by crystal growth of calcite in polyacrylamide gel media (hydrogels).[26,27] In both cases, days to weeks were necessary because reactant diffusion was typically imposed in the experimental setups, which were initially designed to mimic bio-mineralization processes. In this context, studies are designed with a view to improving existing methods and/or developing innovative routes to obtain well-controlled shapes and sizes of calcite mesocrystals. Moreover, these fundamental approaches provide complementary insights into the bio-mineralization processes, as mesocrystals of calcite are found for example in red corals[28] and in brachiopods.[29]

In the present study, we re-investigate calcite formation from $CO_2$–$H_2O$–$Ca(OH)_2$ slurry in order to synthesize porous calcite mesocrystals. Porous mesocrystals of calcite could be used as anti-acid or excipient agents in drugs for human or animals. For this purpose, various common domestic drinks (soluble coffee, orange juice, carrot juice, milk, sugar water and white wine) were used as additives because they are widely available and easily commercialized. We demonstrate herein that porous mesocrystals of calcite with a high specific surface area (up to 30 m$^2$ g$^{-1}$) and peanut-like morphology of aggregates can be obtained except when sugar and milk are used as additives. Only a few hours (<24 h) are required for a complete synthesis, which is possible when using a triphasic gas–liquid–solid system under non-constant high $CO_2$ pressure (anisobaric conditions), contrary to available methods requiring days or weeks and in which reactant diffusion is typically imposed.[24–27] *In situ* monitoring of pH in the interacting solution and of $CO_2$ consumption during the formation of calcite mesocrystals provides further kinetic insights with respect to calcite formation in the absence of additives. To summarize, this study proposes a simple and innovative way of synthesizing porous calcite mesocrystals of regular size and morphology with a high specific surface area. This procedure can be easily extended to industrial scale.

## 2. Materials and methods

### 2.1. Synthesis of nano-sized calcite particles

600 ml of high-purity water with an electrical resistivity of 18.2 MΩ cm and 37 g of commercial calcium hydroxide (provided by Sigma-Aldrich) with 96% chemical purity (3% $CaCO_3$ and 1% other impurities) were placed in a titanium reactor (autoclave with an internal volume of 1 L). The calcium hydroxide particles were immediately dispersed by mechanical agitation (400 rpm) and $CO_2$ (provided by Linde Gas S.A.) was then injected at 55 bar into the reactor at room temperature (20–25 °C). Following injection (≈2 minutes), the temperature variation due to exothermicity, the pH in the interacting solution and $CO_2$ consumption (pressure drop) were monitored *in situ* during calcite nucleation and growth. Temperature and pH are systematically stabilized in the first two hours while the pressure drop related to $CO_2$ consumption takes about 8 hours to stabilize. For this reason, the duration of the reaction was arbitrarily set to 24 h in all the experiments.

At the end of the experiment, the residual $CO_2$ was degassed from the reactor by opening the gas line valve. After degassing for 3–5 minutes, the autoclave was disassembled, and the solid product was carefully recovered and separated by centrifugation (30 min at 12 000 rpm). Finally, the solid product was dried directly in the centrifugation flasks at 90 °C for 48 h. The dry solid product was stored in plastic flasks for subsequent characterization (FESEM, XRD, and $N_2$ sorption isotherms).

### 2.2. Synthesis of porous calcite mesocrystals

To obtain porous calcite mesocrystals with a peanut-like morphology, 5 or 20 g of commercial soluble coffee containing 7.8% of proteins, 3% of sugar and 34.1% of vegetable fibers were added as additives to calcite synthesis. The operating conditions are identical to those used to obtain nano-sized calcite particles (see above sub-section 2.1) except the solid product recovery procedure. In this case, the solid product was washed once by re-dispersion/centrifugation processes in order to remove roughly the soluble residual additive.

Various other common drinks such as pulp-free orange juice (100 ml + 500 ml of high-purity water), pulp-free carrot juice (100 ml + 500 ml of high-purity water) , full-fat milk (100 ml + 500 ml of high-purity water), sugar water (50 g in

600 ml of high-purity water) and commercial white wine (600 ml containing 10% v/v of alcohol) that contain different amounts of proteins, sugars and fibers were also explored as additives in the calcite synthesis. Calcite synthesis in the absence and in the presence of additives and some results are summarized in Table 1. It should be noted that this study does not claim to investigate the influence of a given model macromolecule as systematically proposed in several studies. In fact, we only selected various common drinks containing organic matter of different origins in order to assess their influence on the crystal morphology, crystal size and aggregation state of calcite.

## 2.3. Semi-continuous experiments

A semi-continuous system (sampling of reacting suspension with time) was performed in order to measure the spectral Raman feature (RAMAN RXN1, Kaiser Optical Systems) of collected-time suspensions. For this case, about 25 ml of suspension was sampled in the reactor as a function of time (0, 2, 10, 20, 60 and 120 min) during calcite formation. The P–T conditions were the same as cited above, but, the Raman measurements were carried out in depressurized suspensions. Herein, we assume that the instantaneous depressurization process has small impact on the precipitating particles contained in the collected-time suspensions and we also assume that the carbonation reaction of residual portlandite is stopped.

## 2.4. Characterization of solid products

X-Ray Powder Diffraction (XRD) analyses were performed using a Siemens D5000 diffractometer in Bragg–Brentano geometry, equipped with a theta–theta goniometer with a rotating sample holder. The XRD patterns were collected using Cu $K\alpha_1$ ($\lambda_{K\alpha1}$ = 1.5406 Å) and $K\alpha_2$ ($\lambda_{K\alpha2}$ = 1.5444 Å) radiation in the range $2\theta$ = 10–70° with a step size of 0.04° and a counting time of 6 seconds per step. Calcite formed on experimental XRD patterns was systematically refined by the Rietveld method using the BGMN software and its associated database.[30]
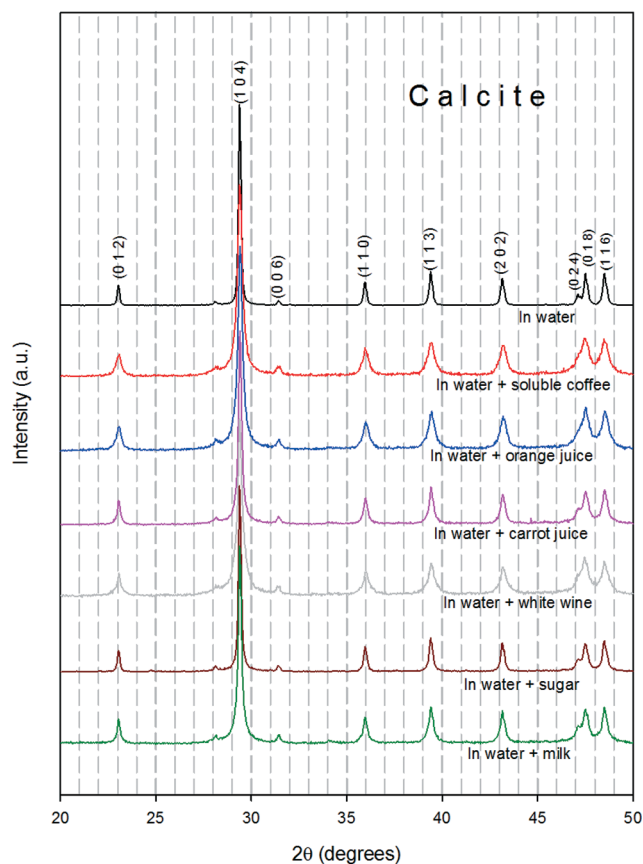


Fig. 1 Experimental XRD patterns for calcite formation *via* aqueous carbonation of portlandite with compressed $CO_2$ in the presence of common domestic drinks. The reflections indicated concern only calcite from ICDD 005-0586.

**FESEM observations.** Solid products were dispersed by ultrasonic treatment in absolute ethanol for five to ten minutes. One or two droplets of the suspension were then deposited directly on an aluminum support for SEM observations, and coated with platinum. The morphology of the crystal faces was observed by using a Zeiss Ultra 55 field emission gun scanning electron microscope (FESEM) with a maximum spatial resolution of approximately 1 nm at 15 kV.

**Table 1** Summary of experimental conditions, mineral composition and some textural properties of solid products

| System | Addt | $P_{CO_2}$ (bar) | | $T$ (°C) | | *In situ* pH | | Mineral/morpho | Size (nm) | | $S_{BET}$ |
| | | Init | Final[a] | $T_{inj.}$ | $T_{max}$ | Init | Final[b] | | XRD | FESEM | $m^2 g^{-1}$ |
|---|---|---|---|---|---|---|---|---|---|---|---|
| P–W–$CO_2$ | None | 55 | 21.5 | 27 | 34 | 12.45 | 4.51 | Calcite/S–R–IA | 81 | 90 | 11 |
| P–W–$CO_2$ | Coffee | 55 | 19.5 | 22 | 29 | 12.59 | 5.19 | Calcite/peanut | 21 | 30 | 30 |
| P–W–$CO_2$ | Orange juice | 55 | 11.5 | 21 | 25 | 12.47 | 5.27 | Calcite/peanut | 23 | 40 | 22 |
| P–W–$CO_2$ | Carrot juice | 55 | 21 | 25 | 29 | 13.10 | 5.13 | Calcite/peanut | 35 | 45 | 16 |
| P–W–$CO_2$ | White wine | 55 | 22 | 27 | 32 | 12.75 | 5.11 | Calcite/peanut | 20 | 25 | 13 |
| P–W–$CO_2$ | Sugar | 55 | 17 | 26 | 31 | 12.59 | 4.95 | Calcite/R–IA | 49 | 55 | 6 |
| P–W–$CO_2$ | Milk | 55 | 20.5 | 24 | 27 | 12.63 | 5.05 | Calcite/R–IA | 31 | 50 | 4 |

P: portlandite ($Ca(OH)_2$); W: high-purity water; Addt: additive; Init: initial; $P_{CO_2}$: pressure of $CO_2$.[a] $CO_2$ pressure after 24 h; $T$: temperature (error = ±1 °C); $T_{inj.}$: temperature at which the $CO_2$ was injected in the system; $T_{max}$: maximum temperature reached by exothermicity. [b] *In situ* pH after 24 h (error = ±0.2); Morpho: morphology; S: scalenohedral; R: rhombohedral; IA: irregular aggregates; peanut: calcite mesocrystals with peanut-like morphology (porous or non-porous); $S_{BET}$: specific surface area (error = ±1 $m^2 g^{-1}$). Error$_{XRD}$ = 10% (numerical error); error$_{FESEM}$ = 5 nm (standard deviation for 50 measures).
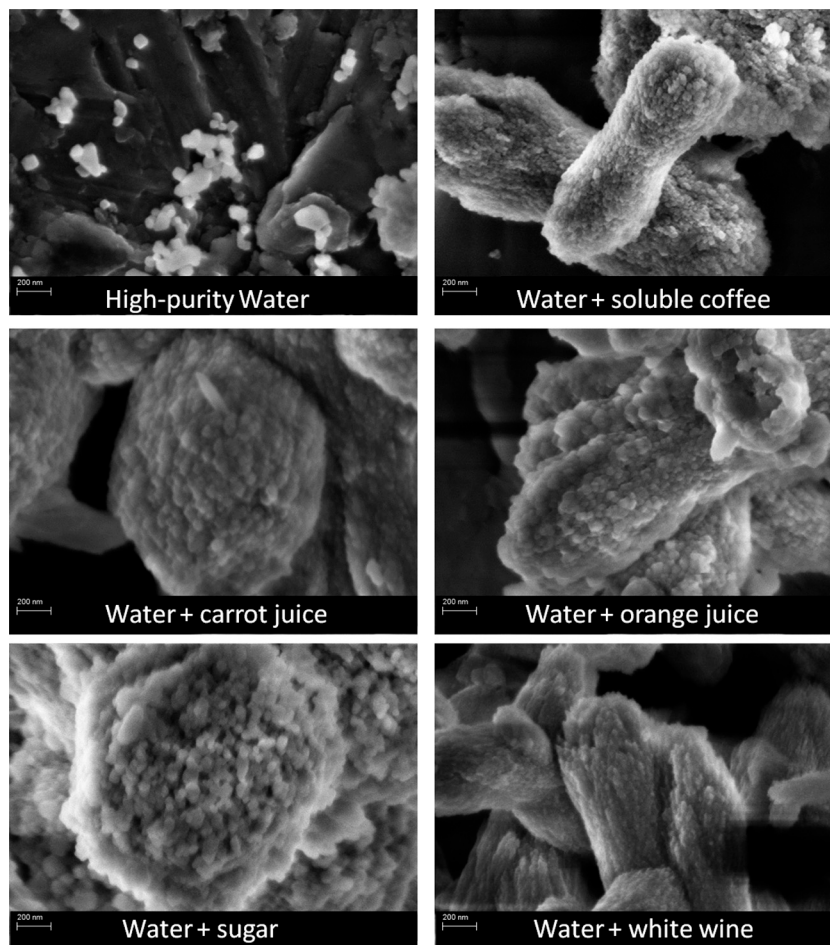
**Fig. 2** FESEM images at the same magnification showing the size and organization of calcite nanoparticles synthesized in the absence and in the presence of domestic drink additives. Calcite mesocrystals with a peanut-like morphology are observed when soluble coffee, orange juice, carrot juice and white wine were used as additives.

**TEM observations.** Calcite mesocrystals synthesized in the presence of soluble coffee were shaken in ethanol for a short time in order to split the aggregates without any additional treatment. A drop of the suspension was deposited on a perforated carbon foil and placed on a conventional copper micro-grid for further observations with a JEOL 2100F Transmission Electron Microscope (TEM) operating at 200 kV, equipped with a field emission gun and a high-resolution pole piece achieving a point-to-point resolution of 1.8 Å. Chemical mapping was achieved by combining the scanning module of the microscope (STEM) with the EDS detector.

**$N_2$ sorption isotherms.** $N_2$ sorption isotherms for calcite samples were determined using a sorptomatic system (Thermo Electron Corporation). The specific surface area of powdered samples was estimated by applying the Brunauer–Emmet–Teller (BET) equation in the $0.05 \leq P/P_0 \leq 0.35$ interval of relative pressure and using a value of 16.2 Å$^2$ for the cross-sectional area of molecular $N_2$. A non-linear regression by the least-squares method was performed to fit the interval data ($n_{ads}$ *vs.* $P/P_0$) in the experimental isotherms. Additionally, the Barrett–Joyner–Halenda (BJH) method, that takes

into account capillary condensation *via* the Kelvin equation, was used to determine pore size distribution.

**Raman spectroscopy.** Raman spectra were measured with a RAMANRXN1 instrument from Kaiser Optical Systems. The spectra were recorded using a Laser wavelength of 785 nm in a spectral range from 400 to 3400 cm$^{-1}$. The spectral resolution was 4 cm$^{-1}$ and 200 scans were collected.

## 3. Results and discussion

In previous studies, it was demonstrated that scalenohedral calcite nanocrystals (<100 nm) are systematically precipitated at low temperature (≤30 °C) *via* aqueous carbonation of portlandite with compressed $CO_2$ under isobaric or anisobaric conditions.[11,31,32] In the present study, similar carbonation experiments were performed at room temperature, and various common domestic drinks (soluble coffee, orange juice, carrot juice, white wine, sugar water and milk) were now used as additives with a view to synthesizing calcite mesocrystals, since this nanostructured material could offer unique new possibilities of usage in industry.[17,20] Moreover,
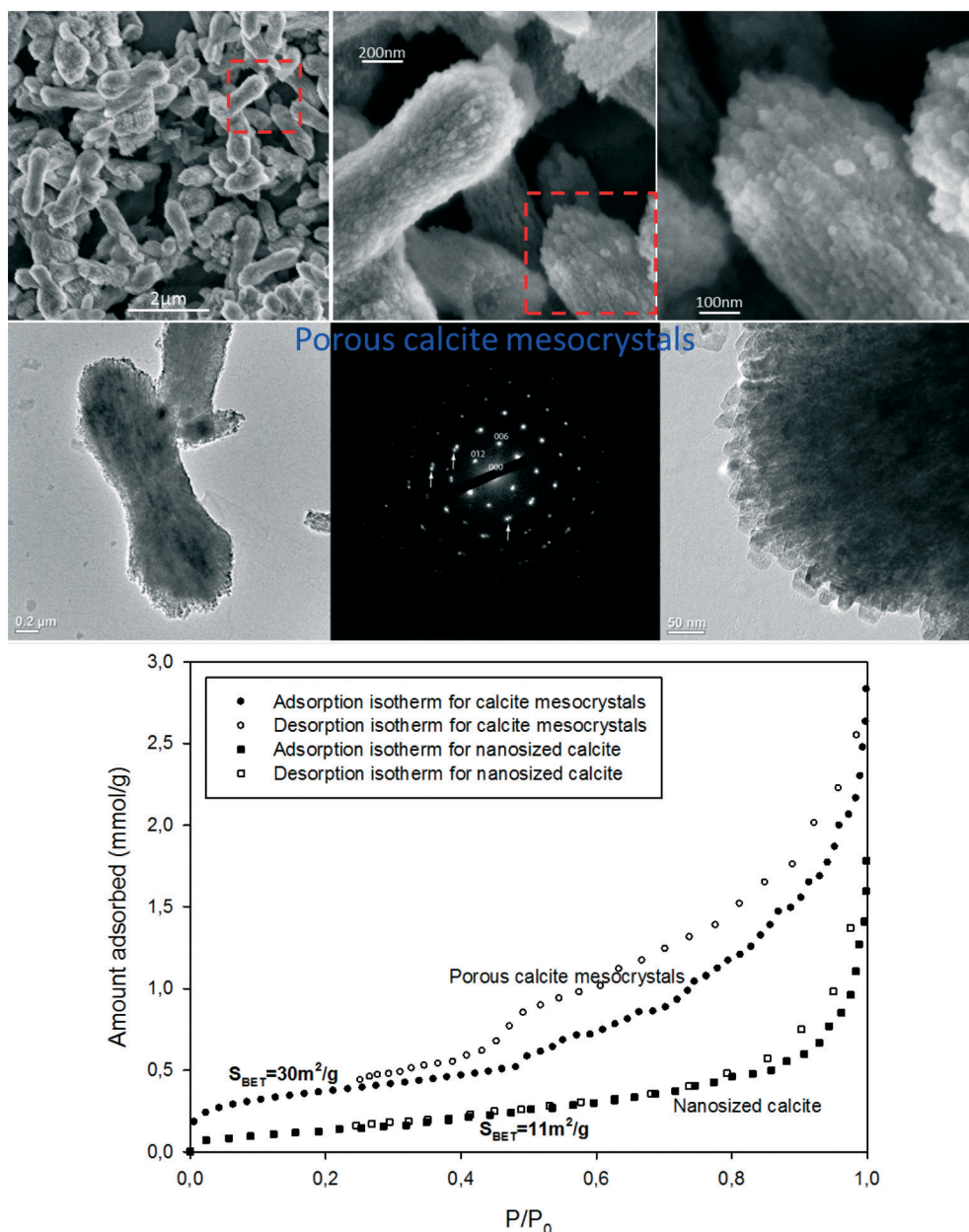
**Fig. 3** Characterization of calcite mesocrystals synthesized in the presence of soluble coffee additive. FESEM images at different magnifications (up); TEM images and SAED pattern acquired on several tens of crystals. Arrows show a slight disorientation (middle); and $N_2$ adsorption–desorption isotherms (bottom).

this simple crystallization system shows how daily additives can change a complete morphosynthesis.

Here, experimental XRD patterns revealed that calcite is the only crystalline component in all the products (Fig. 1), *i.e.* that high concentrations of organic matter (proteins, sugars and fibers) in the system did not induce polymorphism, as often invoked in homogeneous or diffusion systems where ACC, vaterite and/or aragonite were observed at the early stages or co-existed with calcite in the final product.[22,33–36] In fact, from the Rietveld refinement of XRD patterns, only smaller calcite particles (coherent domain average size <50 nm) were produced in the presence of a given

additive with respect to calcite synthesized in the absence of additive, where the coherent domain average size is equivalent to 81 nm. These results concerning the particle size of calcite are in agreement with FESEM observations. However, particle organization at the aggregate scale is very different when additives are used. Clearly, the use of common domestic drinks as additives induced the formation of calcite mesocrystals with a peanut-like morphology except in the case of sugar–water and milk, *i.e.* the formation of a nanostructured material in which the constituent calcite nanoparticles (10 < size < 50 nm) are aligned and/or oriented, forming regular micrometric 3D porous aggregates (<3 μm) (see Fig. 2). In
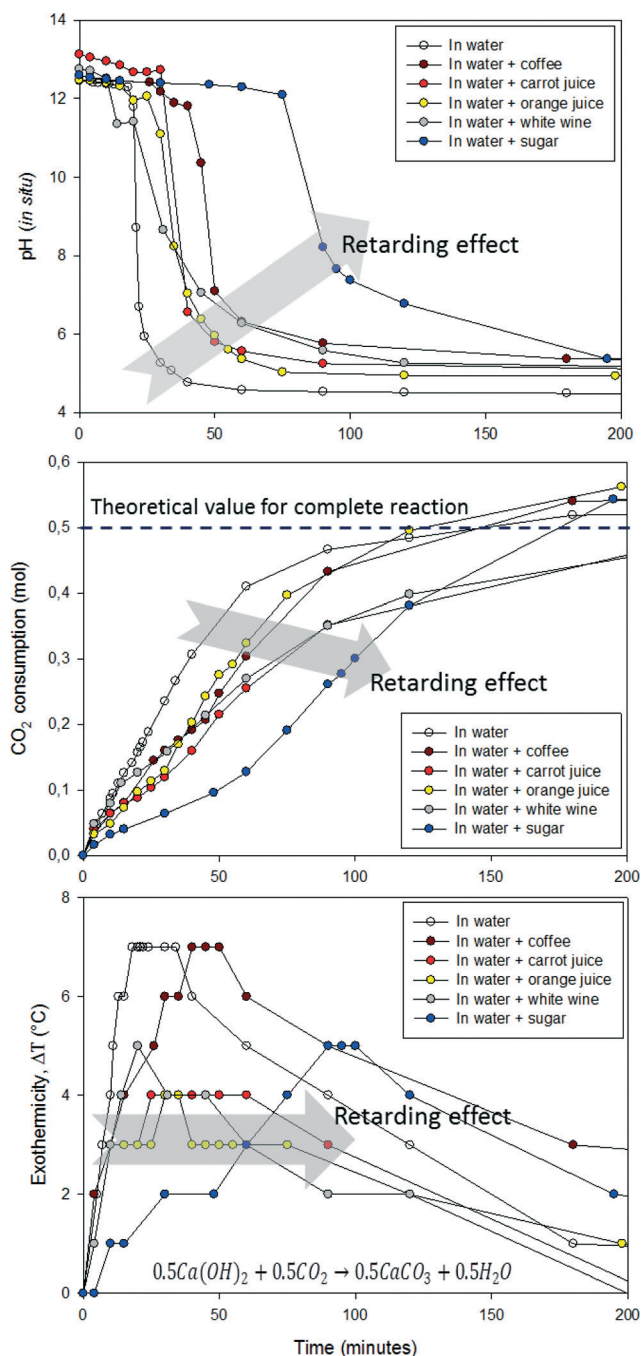
Fig. 5 Experimental kinetic data and fitting curves for $CO_2$ consumption during calcite synthesis. All fitting parameters are summarized in Table 2.

Fig. 4 *In situ* monitoring of pH in the interacting solution (top), $CO_2$ consumption related to $CO_2$ pressure drop (middle), and carbonation exothermicity (bottom).

the case of sugar–water and milk additives, the organization of the calcite nanoparticles is unclear; here, irregular aggregates mixed with well-faceted rhombohedral calcite particles are dominant in the solid products. These results suggest that the orientation of calcite nanocrystals is particularly induced by the presence of vegetable fibers contained in coffee, orange and carrot juices and wine. The mesocrystals produced can be porous nanostructured materials, or nonporous if organic molecules completely fill the existing space
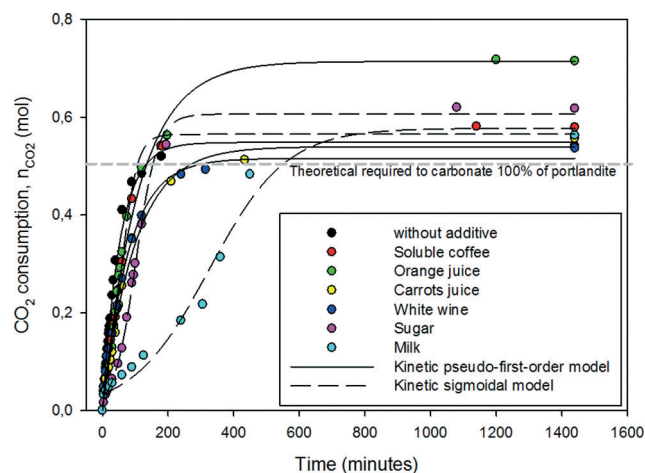
between the primary nanoparticles. Conventional TEM observations thus did not clearly reveal any porosity in the calcite mesocrystals, but the selected area electron diffraction (SAED) pattern in Fig. 3 (middle) confirms that aggregates of calcite nanoparticles with the same orientation form the so-called mesocrystals or pseudo-single calcite crystals (case: coffee as additive). In a complementary context, $N_2$ adsorption isotherms have unambiguously confirmed that calcite mesocrystals obtained in the presence of soluble coffee are porous, as attested by pronounced hysteresis between adsorption–desorption isotherms (see bottom of Fig. 3). Moreover, a high specific surface area of 30 m$^2$ g$^{-1}$ was determined using the BET method and small mesopores of ~7 nm (median pore diameter) were determined using the BJH method. Additional results concerning the average particle size, morphology and specific surface area of all calcite products obtained are reported in Table 1.

*In situ* monitoring of pH in the interacting solution, $CO_2$ consumption (or $CO_2$ pressure drop) and exothermicity provide original and complementary macroscopic kinetics data on the aqueous carbonation of portlandite with compressed $CO_2$ ($Ca(OH)_2 + CO_2 \rightarrow CaCO_3 + H_2O$) in the absence or presence of a given additive (see Fig. 4). In general, the additives investigated produced a complex retarding effect on the carbonation reaction with respect to calcite synthesized in the absence of any additive. This means that the dissolution rate of $CO_2$ was significantly reduced by the presence of a given additive. This macroscopic retarding effect was already observed for calcite formation in presence of oxyanions (or polyatomic ions) in similar experiments.[37] We note that in our system the $CO_2$ dissolution rate, implying both absorption and dissociation processes ($CO_{2(gas)} \rightarrow CO_{2(aq)}$; $CO_{2(aq)} + H_2O \rightarrow HCO_3^- + H^+$ and $HCO_3^- \rightarrow CO_3^{2-} + H^+$), is the limiting step for carbonation of available portlandite – see ref. 10. Portlandite ($Ca(OH)_2$) is initially in excess (61.6 g L$^{-1}$) with respect to its solubility (1.73 g L$^{-1}$ at 20 °C), and consequently this strong base maintains a high pH (>12) after $CO_2$

**Table 2** Summary of kinetic parameters and dissipated heat in the case of aqueous carbonation of portlandite with compressed $CO_2$ in the presence of additives

| Additive | $t_c$ min | First[a] | | Sigmoidal[b] | | | $\Delta T_{max}$ °C | Heat kJ mol$^{-1}$ | RF |
|---|---|---|---|---|---|---|---|---|---|
| | | $n_{max}$ (mol) | $1/k$ (min) | $n_{max}$ (mol) | $k_s$ | $t_{1/2}$ (min) | | | |
| Without | 60 | 0.55 ± 0.01 | 53.13 ± 2 | — | — | — | 7 | 35.20 | — |
| Soluble coffee | 90 | — | — | 0.56 ± 0.01 | 23.98 ± 1.87 | 56.71 ± 2.16 | 7 | 35.20 | 0.05 |
| Orange juice | 75 | 0.71 ± 0.02 | 110 ± 4.85 | — | — | — | 4 | 20.11 | 0.38 |
| Carrot juice | 90 | 0.54 ± 0.01 | 99.38 ± 4.94 | — | — | — | 4 | 20.11 | 0.48 |
| White wine | 120 | 0.51 ± 0.01 | 79.40 ± 4.40 | — | — | — | 5 | 25.14 | 0.38 |
| Sugar | 300 | — | — | 0.60 ± 0.01 | 32.74 ± 1.63 | 101.55 ± 1.82 | 5 | 25.14 | 0.43 |
| Milk | 450 | — | — | 0.57 ± 0.02 | 116.92 ± 11.57 | 325.41 ± 18.10 | 3 | 15.10 | 0.83 |

$t_c$: pH stabilization time after sudden drop (experimental value); First: kinetic pseudo-first-order model used to fit kinetic data from 0 to 24 h.[a] Correlation factor $R = 0.99$; $n_{max}$: maximum amount (in mol) of $CO_2$ transferred from gas phase to suspension (macroscopic equilibrium); $k$: kinetic constant; Sigmoidal: kinetic sigmoidal model used to fit kinetic data from 0 to 24 h. [b] Correlation factor $R = 0.99$; $k_s$: parameter related to the slope of the curve; $t_{1/2}$: time required to reach $n_{max}/2$; $\Delta T$: maximum change in suspension temperature; Heat: heat dissipated by carbonation exothermicity; RF: retarding factor ($0 < RF < 1$) (refer also to Montes-Hernandez et al., 2009 (ref. 37)).

injection until it is completely transformed or carbonated. This critical point (at a given time, $t_c$) is reflected by a sudden drop in pH in the experiments. However, as mentioned above, the additives investigated retard $CO_2$ transfer from gas phase to suspension and, in some cases (coffee–water, sugar–water and milk), the kinetic regime also changed from pseudo-first-order behavior to sigmoidal behavior, as shown in Fig. 5. Herein, a dimensionless retarding factor (RF) was calculated in terms of initial rate as follows: $RF = 1 - v_{0,calcite-drink}/v_{0,calcite}$ where $v_{0,calcite-drink}$ represents the initial rate of $CO_2$ transfer during calcite formation in presence of a given drink (mol s$^{-1}$) and $v_{0,calcite}$ represents the initial reference rate of $CO_2$ transfer only during calcite formation (mol s$^{-1}$), i.e. without additive. More specific details on this simple calculation were already reported by Montes-Hernandez et al.[37] For this simple macroscopic interpretation, retarding effect exist if $0 < RF < 1$, when $RF = 0$ (not retarding effect), $RF = 1$ (complete inhibition reaction) and $RF < 0$ (accelerating affect). For our experiments, all calculated values (Table 2) suggest a retarding effect as claimed above; however, when orange juice was used a higher $CO_2$ consumption at equilibrium was measured suggesting complementary reactions between aqueous $CO_2$ and suspension, probably, the high levels of citrate may form calcium citrate. We note that carbonation exothermicity also experiences a similar retarding effect that is systematically proportional to $CO_2$ consumption; additionally, the additives investigated (except soluble coffee) also produce a reduction in dissipated heat ($q = mc\Delta T$) if pure water is considered in the system. All the experimental and calculated data (including fitting parameters for the kinetic curves reported in Fig. 5) are summarized in Table 2.

Theoretically, the fact that the pH stabilizes after suddenly dropping indicates that portlandite has been completely transformed or carbonated. A simple mass balance reveals that portlandite transformation is non-equimolar with $CO_2$ consumption, since the theoretical $CO_2$ value (in mol) required to carbonate the available portlandite is reached slowly after about 2.5 h in the case of calcite synthesis in the absence of additive, while complete transformation takes place after about 1 h as indicated by the sudden drop and stabilization of pH. This discrepancy could be explained by the formation of transient complex ionic or non-ionic species or by transient portlandite interactions with nucleating calcite nanoparticles. In both cases the formation of colloidal suspensions is expected at the early stage of carbonation. Similar behavior was observed in the case of calcite synthesis in the presence of a given additive (see photographs on the upper part of Fig. 6). In this context, preliminary direct Raman measurements on sampled suspensions as a function of time in the case of calcite synthesis in the absence of additive reveal direct calcite nucleation from the colloidal suspension (Fig. 6: bottom), as already simulated by using the classical crystallization pathway.[10] In other words, ACC is not the exclusive and universal precursor of calcite formation, as recently proposed by Hu et al.[8] However, to confirm this assumption, a real-time Raman analysis under high $CO_2$ pressure is required. Following the same reasoning, the calcite mesocrystals produced using organic additives can also be formed via the classical crystallization pathway, but now assuming that nucleating calcite nanoparticles are rapidly oriented by intercalation of organic matter or directly nucleated on the preexisting oriented sites in the organic matrix (mainly in vegetable fibers), leading to 3D calcite mesocrystals in our experiments. Unfortunately, this orientation mechanism cannot directly measured/observed from our experimental setup. We note that the formation of mesocrystals (including particle orientation mechanism) is still an open subject in the materials science (including biomineralization).

## 4. Conclusion

The controlled synthesis of mesocrystals has been attracting considerable attention in the material sciences community in recent years, since they offer unique new opportunities for material design due to their mesoscopic structure. Here, we
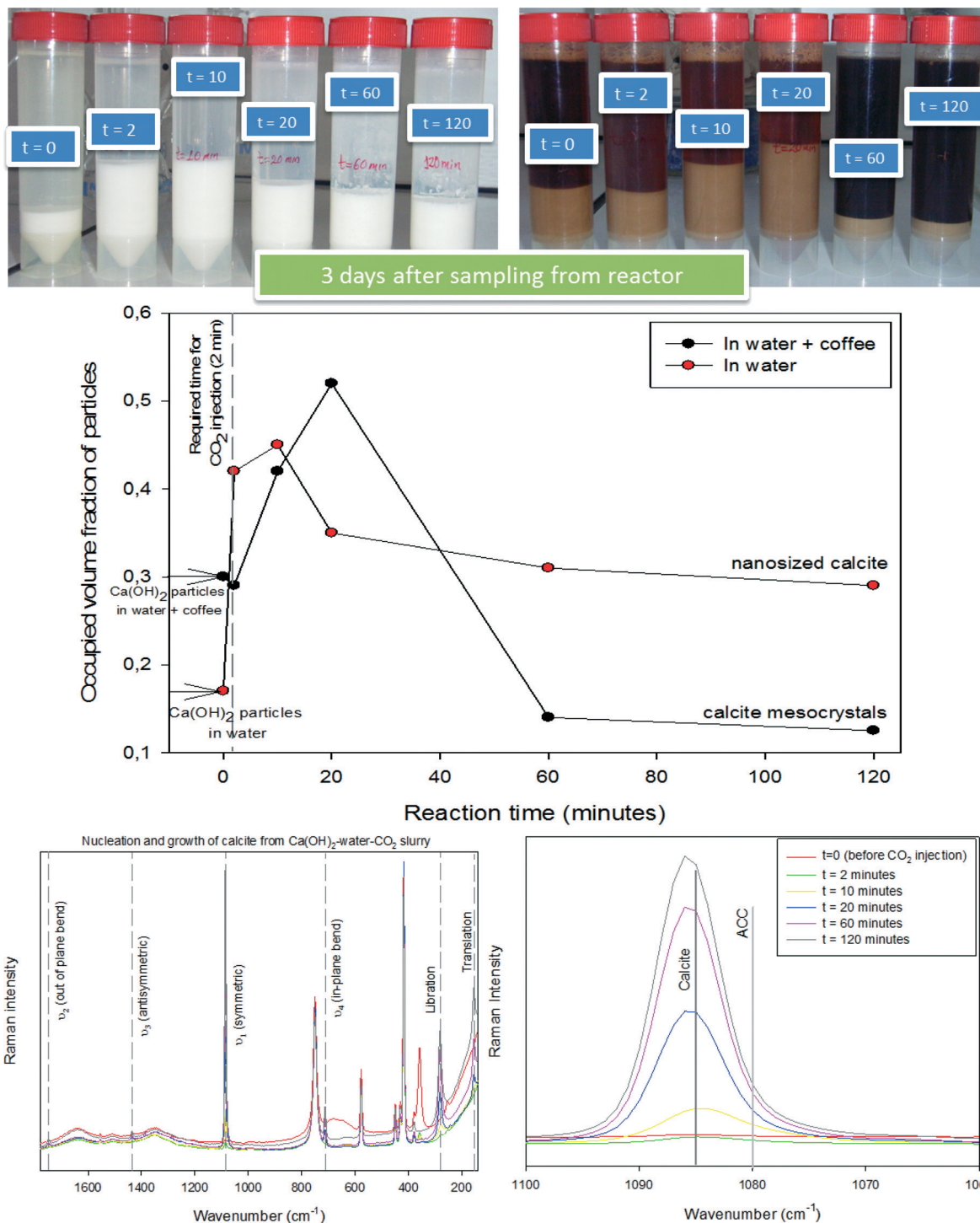
Fig. 6 Static-natural sedimentation (after 3 days) of suspensions sampled during calcite formation without additive and in the presence of soluble coffee (top); apparent occupied volume fraction as a function of reaction time, roughly showing that smaller particles are formed at the early stages of calcite formation (middle); direct Raman measurements on the sampled suspension showing classical crystallization pathway for calcite synthesis without additive.

propose a simple and innovative method for synthesizing porous calcite mesocrystals than could offer new possibilities of usage in industry or improve the existing industrial and medical uses of powdered synthetic calcite. Two main advantages are claimed. Firstly, common domestic drinks can be

used as additives, leading to excellent orientation of the calcite nanoparticles (10–50 nm) to form regular micrometric (<3 μm) 3D porous aggregates with a peanut-like morphology and high specific surface area (up to 30 $m^2$ $g^{-1}$). Secondly, only a few hours (6 h < time < 24 h) are required and

synthesis is possible using a dispersed triphasic gas–liquid–solid system under high non-constant $CO_2$ pressure (anisobaric conditions). In addition, our proposed synthesis procedure could easily be extrapolated to industrial scale.

## Acknowledgements

## References

1 J. Paquette and R. J. Reeder, *Geochim. Cosmochim. Acta*, 1995, **59**, 735–749.

2 S. L. S. Stipp, J. T. Christensen, L. Z. Lakshtanov, J. A. Baker and T. Waight, *Radiochim. Acta*, 2006, **94**, 523–528.

3 Y. Y. Kim, L. Ribeiro, F. Maillot, O. Ward, S. J. Eichhorn and F. C. Meldrum, *Adv. Mater.*, 2010, **22**, 2082–2086.

4 J. L. Bischof, *J. Geophys. Res.*, 1968, **73**, 3315–3322.

5 G. H. Nancollas and M. M. Reddy, *J. Colloid Interface Sci.*, 1971, **37**, 824–830.

6 H. H. Teng, P. M. Dove, C. A. Orme and J. J. De Yoreo, *Science*, 1998, **282**, 724–727.

7 R. Q. Song, A. W. Xu, M. Antonietti and H. Cölfen, *Angew. Chem., Int. Ed.*, 2009, **48**, 395–399.

8 Q. Hu, M. H. Nielsen, C. L. Freeman, L. M. Hamm, J. Tao, J. R. I. Lee, T. Y. J. Han, U. Becker, J. H. Harding, P. M. Dove and J. J. De Yoreo, *Faraday Discuss.*, 2012, **159**, 509–523.

9 A. J. Giuffre, L. M. Hamm, N. Han, J. J. De Yoreo and P. M. Dove, *Proc. Natl. Acad. Sci. U. S. A.*, 2013, **23**, 9261–9266.

10 B. Fritz, A. Clément, G. Montes-Hernandez and C. Noguera, *CrystEngComm*, 2013, **15**, 3392–3401.

11 G. Montes-Hernandez, A. Fernandez-Martinez, L. Charlet, D. Tisserand and F. Renard, *J. Cryst. Growth*, 2008, **310**, 2946–2953.

12 D. Gebauer, A. Völkel and H. Cölfen, *Science*, 2008, **322**, 1819–1822.

13 L. B. Gower and D. A. Tirrell, *J. Cryst. Growth*, 1998, **191**, 153–160.

14 D. Gebauer, M. Kellermeier, J. D. Gale, L. Bergstrom and H. Colfen, *Chem. Soc. Rev.*, 2014, **43**, 2348–2371.

15 T. Wang, H. Cölfen and M. Antonietti, *J. Am. Chem. Soc.*, 2005, **127**, 3246–3247.

16 T. Wang, M. Antonietti and H. Cölfen, *Chem. – Eur. J.*, 2006, **12**, 5722–5730.

17 R. Q. Song and H. Cölfen, *Adv. Mater.*, 2010, **22**, 1301–1330.

18 L. M. Hamm, A. J. Giuffre, N. Han, J. Tao, D. Wang, J. J. De Yoreo and P. M. Dove, *Proc. Natl. Acad. Sci. U. S. A.*, 2014, **111**(4), 1304–1309.

19 H. Cölfen and M. Antonietti, *Angew. Chem., Int. Ed.*, 2005, **44**, 5576–5591.

20 L. Zhou and P. O'Brien, *J. Phys. Chem. Lett.*, 2012, **3**, 620–628.

21 G. Montes-Hernandez, D. Daval, R. Chiriac and F. Renard, *Cryst. Growth Des.*, 2010, **10**, 4823–4830.

22 G. Falini, *Int. J. Inorg. Mater.*, 2000, **2**, 455–461.

23 F. C. Meldrum, *Int. Mater. Rev.*, 2003, **48**, 187–224.

24 D. Gebauer, A. Verch, H. G. Börner and H. Cölfen, *Cryst. Growth Des.*, 2009, **9**, 2398–2403.

25 W. Li and P. Wu, *CrystEngComm*, 2009, **11**, 2466–2474.

26 O. Graβmann, R. B. Neder, A. Putnis and P. Löbmann, *Am. Mineral.*, 2003, **88**, 647–652.

27 H. Li and L. A. Estroff, *CrystEngComm*, 2007, **9**, 1153–1155.

28 N. Floquet and D. Vielzeuf, *Cryst. Growth Des.*, 2012, **12**, 4805–4820.

29 W. W. Schmahl, E. Grisshaber, K. Kelm, A. Goetz, G. Jordan, A. Ball, D. Xu, C. Merkel and U. Z. Brand, *Kristallografiya*, 2012, **227**, 793–804.

30 T. Taut, J. Bergmann, G. Schreiber, A. Börner and E. Müller, *Mater. Sci. Forum*, 1996, **177–182**, part 1.

31 G. Montes-Hernandez, F. Renard, N. Geffroy, L. Charlet and J. Pironon, *J. Cryst. Growth*, 2007, **308**, 228–236.

32 G. Montes-Hernandez, G. Sarret, R. Hellmann, N. Menguy, D. Testemale, L. Charlet and F. Renard, *Chem. Geol.*, 2011, **290**, 109–120.

33 G. Falini, S. Fermani and A. Ripamonti, *J. Inorg. Biochem.*, 2002, **91**, 475–480.

34 J. Kontrec, D. Kralj, L. Brecevic and G. Falini, *J. Cryst. Growth*, 2008, **310**, 4554–4560.

35 A. Dey, G. De With and J. M. Sommerdijk, *Chem. Soc. Rev.*, 2010, **39**, 397–409.

36 F. Huang, S. Li, J. Song, L. Chen, X. Zhang, Y. Shen and A. Xie, *CrystEngComm*, 2012, **14**, 1277–1282.

37 G. Montes-Hernandez, N. Concha-Lozano, F. Renard and E. Quirico, *J. Hazard. Mater.*, 2009, **166**, 788–795.